FEBS openbio

FEBS PRESS science publishing by scientists

Interaction with adenylate cyclase toxin from *Bordetella pertussis* affects the metal binding properties of calmodulin

Tzvia I. Springer[1], Corey C. Emerson[1,*], Christian W. Johns[2] and Natosha L. Finley[1,2]

1 Department of Microbiology, Miami University, Oxford, OH, USA
2 Cell, Molecular, and Structural Biology Program, Miami University, Oxford, OH, USA

Keywords
adenylate cyclase; calcium; calmodulin; magnesium; nuclear magnetic resonance

Correspondence
N. L. Finley, Cell, Molecular, and Structural Biology Program, Department of Microbiology, Miami University, 700 E. High Street, Oxford, OH 45056, USA
Fax: +1 513 529 2431
Tel: +1 513 529 0950
E-mail: finleynl@miamioh.edu

***Present address**
Department of Pharmacology, Cleveland Center for Membrane and Structural Biology, Case Western Reserve University, Cleveland, OH 44106, USA

(Received 18 April 2016, revised 27 September 2016, accepted 29 September 2016)

doi:10.1002/2211-5463.12138

Adenylate cyclase toxin domain (CyaA-ACD) is a calmodulin (CaM)-dependent adenylate cyclase involved in *Bordetella pertussis* pathogenesis. Calcium (Ca^{2+}) and magnesium (Mg^{2+}) concentrations impact CaM-dependent CyaA-ACD activation, but the structural mechanisms remain unclear. In this study, NMR, dynamic light scattering, and native PAGE were used to probe Mg^{2+}-induced transitions in CaM's conformation in the presence of CyaA-ACD. Mg^{2+} binding was localized to sites I and II, while sites III and IV remained Ca^{2+} loaded when CaM was bound to CyaA-ACD. $2Mg^{2+}/2Ca^{2+}$-loaded CaM/CyaA-ACD was elongated, whereas mutation of site I altered global complex conformation. These data suggest that CyaA-ACD interaction moderates CaM's Ca^{2+}- and Mg^{2+}-binding capabilities, which may contribute to pathobiology.

Bordetella pertussis secretes an adenylate cyclase toxin (CyaA), a critical bacterial virulence factor, which is activated by calmodulin (CaM) during host cell infection. CyaA is composed of a 141 kDa hemolytic C-terminal domain and a 43 kDa N-terminal adenylate cyclase toxin domain (CyaA-ACD) [1,2] When stimulated by CaM, CyaA-ACD converts ATP to cAMP leading to a pathophysiological accumulation of intracellular cAMP [3–5]. Interaction with both N-terminal and C-terminal domains of intact CaM contributes to a 400-fold increase in CyaA-ACD binding affinity as compared to the isolated N-terminal or C-terminal domain, but the molecular mechanism remains to be determined [6]. *In vitro* assays demonstrate that CaM-dependent CyaA-ACD activation occurs at low calcium (Ca^{2+}) (0.1 μM) in the presence of high magnesium (Mg^{2+}) concentrations (0.1–10 mM) [6], conditions under which the metal binding characteristics of these proteins likely contribute to catalysis. Moreover, elevated Ca^{2+} inhibits CyaA-ACD activation, necessitating increased Mg^{2+} concentration for stimulation, but the metal-dependent mechanisms and the roles that CyaA-ACD and CaM play in this process remain to be determined.

Abbreviations
Ca^{2+}, calcium; CaM, calmodulin; CyaA-ACD, adenylate cyclase toxin domain; DLS, dynamic light scattering; Mg^{2+}, magnesium.

Calmodulin is a ubiquitous eukaryotic protein that senses changes in cytosolic Ca^{2+} levels in response to physiological stimuli. As a member of the EF-hand family of proteins, CaM and other Ca^{2+}-responsive proteins, such as troponin C (TnC), have helix-loop-helix structural motifs that ligate Ca^{2+} in response to cellular signaling [7]. In the cell, resting levels of intracellular free Mg^{2+} are maintained in the millimolar range, while Ca^{2+} concentrations fluctuate from 0.1 to 0.5 μM upon stimulation. In order to transmit the signals involved in triggering Ca^{2+}-regulated biological processes, CaM must differentially bind Ca^{2+} and Mg^{2+}.

Calmodulin has four highly conserved Ca^{2+}/Mg^{2+}-binding sites. It is composed of N-terminal and C-terminal globular domains connected by a flexible tether. Sites I and II are in the N-terminal domain while sites III and IV are located in the C-terminal domain of CaM. It is known that both domains of CaM cooperatively bind Ca^{2+} with higher affinity than Mg^{2+}. The C-terminal domain, which is known to play a prominent role in target binding, has higher Ca^{2+} affinity than the N-terminal domain. In contrast, the N-terminal domain binds Mg^{2+} with higher affinity than the C-terminal domain, indicating that preferential metal binding in each domain may have regulatory functions in CaM-dependent activation. In the absence of Ca^{2+}-coordination, the globular domains of CaM are 'closed' (ApoCaM) with minimal exposure of the hydrophobic clefts. Ca^{2+} binding to sites I–IV promotes conformational rearrangements in CaM and subsequent exposure of hydrophobic surface areas in each domain, which is important in target peptide recognition [8]. While Mg^{2+} binding induces smaller, yet distinct structural transitions in CaM [9–12], it is postulated to serve mainly as a suppressor of CaM-dependent activation. In the presence of physiologically relevant Mg^{2+} concentrations, it is reported that Ca^{2+} affinity in CaM diminishes. However, the Mg^{2+}-binding constants in CaM are such that it is likely to be fully or partially Mg^{2+} loaded at resting Ca^{2+} concentrations [12]. The probability of multiple intracellular populations consisting of Mg^{2+}/Ca^{2+}-loaded CaM conformers would suggest that a simple 'on/off' regulatory switch may not be adequate to control CaM-dependent enzyme activation.

Although the molecular mechanisms are unknown, Ca^{2+}-independent and -dependent activation of CyaA-ACD occurs upon interaction with CaM [13]. To date, there is no high-resolution structure of intact CaM bound to CyaA-ACD, so the role of metal binding in the catalytic stimulation of this system remains obscure. A functionally homologous adenylate cyclase toxin made by *Bacillus anthracis* (EF) engages the N-terminal domain of CaM through extensive intermolecular contacts with the helical domain. However, N-terminal CaM remains in a closed conformational state when associating with EF and requires elevated Ca^{2+} for activation [14–16]. In direct contrast, CaM-dependent activation of CyaA-ACD occurs at lower Ca^{2+} concentrations and is not regulated by intracellular Ca^{2+} concentration [6,17,18]. N-terminal CaM is required for full activation even though CaM mutants defective in N-terminal domain opening also activate CyaA-ACD [6]. The N-terminal domain of CaM has a unique conformational state upon CyaA-ACD association that does not resemble 'closed' CaM [19]. Furthermore, we showed that N-terminal CaM directly contacts CyaA-ACD through interactions involving the β-hairpin of CyaA-ACD. Abolishing the intermolecular association between N-terminal CaM and the β-hairpin promotes conformational exchange in metal-binding site II of CaM [19,20]. Clearly, interaction with N-terminal CaM, and metal-induced conformational transitions in CaM, are important factors in controlling CyaA-ACD association, but the structural mechanisms remain unclear. Taken together, the collective evidence points to the possibility that bacterial adenylate cyclase toxins, in particular CyaA-ACD, have evolved novel modes of activation from their eukaryotic counterparts. Exploiting these molecular differences in CaM-dependent adenylate cyclase activation may provide a means by which to develop highly specific, novel therapeutic agents to combat emerging infectious diseases. In our present study, we seek to examine the roles of Mg^{2+} and Ca^{2+} binding in CaM/CyaA-ACD complex formation using NMR, dynamic light scattering (DLS), site-directed mutagenesis, and native PAGE. These findings provide a structural framework from which to consider the potential role Mg^{2+}/Ca^{2+} binding has in CaM-dependent enzyme activation.

Materials and methods

Sample preparation

Recombinant CyaA-ACD was overproduced and purified as previously described [19]. Cell pellets containing insoluble CyaA-ACD were resuspended on ice in buffer containing 8 M Urea, 500 mM NaCl, 40 mM imidazole, 20 mM Tris-HCl, and 1 mM PMSF at pH 8.0 and lysed by sonication. CyaA-ACD was resolved using HisTrapTM HP Ni-Sepharose resin (GE Healthcare, Pittsburgh, PA, USA). Recombinant CyaA-ACD was eluted from columns with increasing concentrations of imidazole and identified as

homogenous as analyzed by SDS/PAGE, as previously described [19]. Bradford assay was used to quantify purified CyaA-ACD.

Recombinant stable isotope labeled and unlabeled CaM were expressed, purified, and quantified as previously described [19]. Site-directed mutagenesis of Glu31Asp in CaM (CaME31D) was performed according to the manufacturer's protocol using the Quikchange™ mutagenesis kit (Santa Clara, CA, USA). Recombinant CaME31D was also expressed, purified, and quantified as previously described [19]. All CaM samples were concentrated using a centricon (Corning, Oneonta, NY, USA) and stored at −20 °C.

ApoCaM was prepared by dialyzing purified recombinant proteins against 4 L of buffer containing 250 mM NaCl, 20 mM EDTA, 20 mM EGTA, 20 mM Hepes-NaOH pH 7.3, and 1 mM PMSF. Fully Mg^{2+}-loaded CaM ($4Mg^{2+}$-CaM) was prepared by dialysis and ultracentricon buffer exchange of ApoCaM into 250 mM NaCl, 40 mM $MgCl_2$, 20 mM Hepes-NaOH pH 7.3, and 1 mM PMSF. Partially $2Mg^{2+}/2Ca^{2+}$-loaded CaM ($2Mg^{2+}/2Ca^{2+}$-CaM) was prepared by dialyzing $4Ca^{2+}$-CaM against 250 mM NaCl, 40 mM $MgCl_2$, 20 mM Hepes-NaOH pH 7.3, and 1 mM PMSF. For all experiments, ultrapure $MgCl_2$ and $CaCl_2$ were used. Complex formation between CyaA-ACD and stable isotope-labeled CaM was performed as previously described [19].

For NMR analyses, samples of [^{2}H, ^{15}N] ApoCaM or [^{2}H, ^{15}N, ^{13}C] ApoCaM ranging in protein concentration between 0.5 and 0.7 mM were suspended in 250 mM NaCl, 1 mM EGTA, 40 mM $MgCl_2$, 20 mM Hepes-NaOH pH 7.3, 1 mM PMSF, and 10%D_2O (NMR buffer). To prepare samples of recombinant $2Mg^{2+}/2Ca^{2+}$-CaM and $2Mg^{2+}/2Ca^{2+}$-CaM/CyaA-ACD, purified proteins consisting of [^{2}H, ^{15}N, ^{13}C] $4Ca^{2+}$-CaM or [^{2}H, ^{15}N, ^{13}C]$4Ca^{2+}$-CaM/CyaA-ACD were exchanged into buffer containing 40 mM $MgCl_2$ using dialysis followed by centricon concentration into NMR buffer.

NMR spectroscopy

NMR experiments were performed on a Bruker Avance III (www.bruker.com) 600 MHz spectrometer equipped with a conventional 5-mm probe. Two dimensional Transverse Relaxation Optimized (^{1}H-^{15}N TROSY-HSQC) spectra were collected for all samples at 298 K. The metal occupancy of each sample was monitored by 2D TROSY-HSQC as each state had a unique spectrum similar to previously published data [19,21,22]. The backbone chemical shift assignments for [^{2}H, ^{15}N, ^{13}C]$2Mg^{2+}/2Ca^{2+}$-CaM/CyaA were determined in part by direct comparison to the previously known values of [^{2}H, ^{15}N, ^{13}C]$4Ca^{2+}$-CaM/CyaA-ACD and confirmed by using the following suite of triple-resonance experiments: ^{15}N edited NOESY-HSQC, TROSY-HNCO, TROSY-HNHA, and TROSY-HNCA. NMR data were processed using NMRPipe [23] analyzed using SPARKY [24]. Amide proton-nitrogen chemical shift perturbations were calculated as described [19].

Dynamic light scattering experiments

Dynamic light scattering measurements were performed on 20 μM samples suspended in NMR buffer (containing 10 mM $CaCl_2$ or 40 mM $MgCl_2$) using the Malvern Zetasizer Instrument (Malvern, Westborough, MA, USA) equipped with a temperature controller. Prior to recording DLS data, samples were centrifuged and filtered to remove particulate matter. Aliquots of 90 μL were dispensed into the small volume cuvette and measurements were collected for $4Ca^{2+}$-CaM, $4Ca^{2+}$-CaM/CyaA-ACD, $2Mg^{2+}/2Ca^{2+}$-CaM/CyaA, and $2Mg^{2+}/2Ca^{2+}$-CaME31D/CyaA-ACD complexes. Data were analyzed using Malvern ZETASIZER software (Malvern).

Native PAGE

Routinely, samples were analyzed following complex formation and size exclusion chromatography (SEC) by native PAGE. For small-scale complex formation, increasing amounts of CyaA-ACD (0–2.5 μM) were titrated into samples of 5 μM CaM or CaM(E31D) in the presence of 250 mM NaCl, 20 mM Hepes-NaOH pH 7.3, and 1 mM PMSF buffer containing either 10 mM $CaCl_2$ or 40 mM $MgCl_2$, respectively. Following incubation at room temperature, samples consisting of free CaM, free CyaA, and CaM/CyaA-ACD complexes were subjected to native PAGE in the presence of 10 mM $CaCl_2$ or 40 mM $MgCl_2$ at 4°C. Proteins were visualized by Coomassie Brilliant Blue staining.

Results and Discussion

Metal binding in N-terminal CaM upon CyaA-ACD association

To investigate the influence of CyaA-ACD association on the metal binding properties of CaM, we monitored Mg^{2+}-induced structural changes in this system by solution NMR, DLS, and native PAGE. We have previously shown that these tools are useful for probing CyaA-ACD-induced conformational transitions in $4Ca^{2+}$-CaM [19]. In the present study, stable isotope labeled CaM was used to generate complexes with unlabeled CyaA-ACD in the presence of Mg^{2+}. Under these conditions, it was determined that the N-terminal domain of CaM is Mg^{2+} loaded in the presence of CyaA-ACD. Given that we were able to clearly distinguish the various metal-ligated states of CaM in the presence and absence of CyaA-ACD, we reasoned that

NMR would permit the observation of conformational changes occurring at each amino acid ligand. The global conformations of $4Ca^{2+}$-CaM/CyaA-ACD and $2Mg^{2+}/2Ca^{2+}$-CaM/CyaA-ACD were similar as evidenced by comparison of 2D ^{1}H-^{15}N TROSY spectra (Fig. 1). Association of CyaA-ACD with CaM occurred in slow exchange on the NMR time scale which permits the determination of resonance assignments for ≥ 85% of the residues in CyaA-ACD-bound CaM complexes. The availability of chemical shift assignments for N-terminal $2Mg^{2+}$-CaM facilitated resonance assignment for $4Mg^{2+}$-CaM [22]. The chemical shift assignments of free $2Mg^{2+}/2Ca^{2+}$-CaM were also based in part on published values. However, significant exchange broadening of residues mapping to the metal-binding sites of CaM was observed for $2Mg^{2+}/2Ca^{2+}$-CaM, most likely a consequence of exchange between ApoCaM and Mg^{2+}-loaded conformers. Upon interaction with CyaA-ACD, Ca^{2+} affinity in C-terminal CaM was increased and, it was possible to monitor Mg^{2+} binding to N-terminal CaM in the $2Mg^{2+}/2Ca^{2+}$-CaM/CyaA-ACD complex. Routinely, it was feasible to directly transfer many of the chemical shift assignments from $4Ca^{2+}$-CaM/CyaA-ACD to $2Mg^{2+}/2Ca^{2+}$-CaM/CyaA-ACD. Verification of sequential resonance assignments was achieved using ^{15}N-edited NOESY-HSQC experiments collected at 70- and 150-ms mixing times. The backbone Cα and C′ resonances were correlated with ^{1}H and ^{15}N amide residues using multidimensional, heteronuclear NMR experiments. Observed backbone chemical shift values were similar to $4Ca^{2+}$-CaM/CyaA-ACD, indicating that Mg^{2+} binding does not significantly alter the secondary structure of CaM in the presence of CyaA-ACD.

Comparison of the ^{1}H-^{15}N TROSY spectra of [^{2}H, ^{15}N, ^{13}C]$2Mg^{2+}/2Ca^{2+}$-CaM/CyaA and [^{2}H, ^{15}N, ^{13}C] $4Ca^{2+}$-CaM/CyaA-ACD revealed Mg^{2+} binding is limited to N-terminal CaM in the presence of CyaA-ACD (Fig. 1). For example, the amide proton-nitrogen resonances for T29 and I27, mapping to site I in N-terminal CaM, exhibited metal-specific conformations in the $2Mg^{2+}/2Ca^{2+}$-CaM/CyaA-ACD and $4Ca^{2+}$-CaM/CyaA-ACD complexes (Fig. 1A). NMR

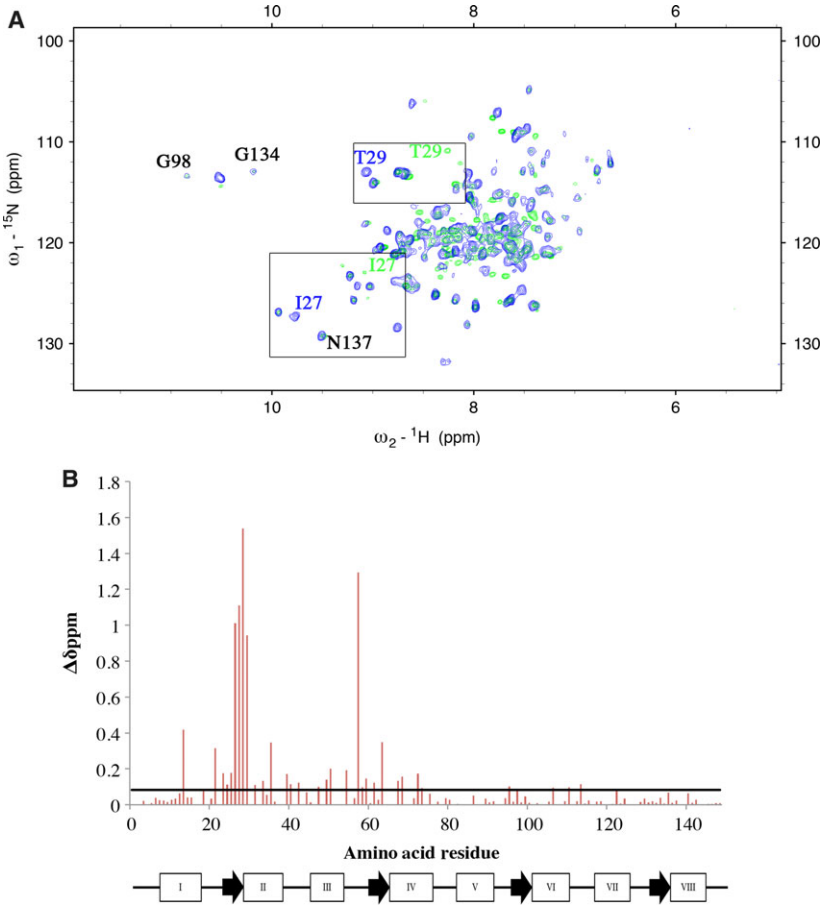

Fig. 1. Comparison of 2D ^{1}H-^{15}N TROSY spectra revealing that Mg^{2+} binding is localized to sites I and II in the CaM/CyaA-ACD complex. (A) [^{15}N, ^{13}C, ^{2}H]-CaM bound to CyaA-ACD in the presence of $4Ca^{2+}$ saturation (blue) and $2Mg^{2+}/2Ca^{2+}$ saturation (green). Selected residues are labeled according to the amino acid residue. (B) Amide proton-nitrogen chemical shift differences mapping to residues in [^{15}N, ^{13}C, ^{2}H]-CaM/CyaA-ACD that are perturbed by Mg^{2+} binding to sites I and II. The secondary structure of CaM is summarized with rectangles (helices) and arrows (β-sheets). The average chemical shift change + one standard deviation is indicated by the horizontal black line. The observation of overlapping resonances mapping to the C-terminal domain of CaM in both the $4Ca^{2+}$-CaM-CyaA-ACD and $2Mg^{2+}/2Ca^{2+}$-CaM/CyaA-ACD complexes indicates that sites III and IV remain Ca^{2+} loaded. In contrast, the amide proton-nitrogen resonances in the N-terminal domain have Mg^{2+}-specific conformations in the $2Mg^{2+}/2Ca^{2+}$-CaM/CyaA-ACD complex.

chemical shift mapping revealed that Mg^{2+} binding is localized to sites I and II in the $2Mg^{2+}/2Ca^{2+}$-loaded complex (Fig. 1B). The residues involved in Mg^{2+} ligation and their corresponding chemical shift values were similar to those reported for free N-terminal CaM [22]. It has been shown that the smaller ionic radius of the Mg^{2+} ion has different coordination geometry than the larger Ca^{2+}, which limits the conformation plasticity in EF-hand proteins [12,22]. Additionally, we found that residues mapping to sites I and II were perturbed in a way that is indicative of Mg^{2+} ion coordination at each metal-binding loop. It is known that NMR chemical shift values of residues at positions 8 of the metal-binding loops in Ca^{2+}- or Mg^{2+}-loaded CaM are useful indicators of the metal occupancy [22,25]. Consistent with this, the amide nitrogen chemical shift differences at positions I27 and I63 in $2Mg^{2+}/2Ca^{2+}$-CaM/CyaA-ACD were shifted +11.0 and +4.1 p.p.m., respectively, compared to ApoCaM (data not shown). The magnitude of the amide chemical shift differences were less substantial at positions 8 in site I and II of $2Mg^{2+}/2Ca^{2+}$-CaM/CyaA-ACD than that observed in the fully loaded Ca^{2+} complex which likely reflects that CyaA-association promotes a less 'open' conformational state in N-terminal CaM. These findings are indicative of CaM being a structurally dynamic Ca^{2+}-sensing protein, a property which is known to function in metal binding and target recognition [26–28]. Taken together, these data support that $2Mg^{2+}$ ions are bound to N-terminal CaM in the presence of CyaA-ACD.

In contrast, sites III and IV in $2Mg^{2+}/2Ca^{2+}$-CaM/CyaA-ACD were not affected by the presence of Mg^{2+}, showing that Ca^{2+} remains bound to C-terminal CaM. Resonances G98 and N137 mapping to the C-terminal CaM were overlapped in the TROSY spectra of $2Mg^{2+}/2Ca^{2+}$-CaM/CyaA-ACD and $4Ca^{2+}$-CaM/CyaA-ACD complexes, which suggests that the C-terminal domain remains Ca^{2+} loaded in these complexes (Fig. 1A). No detectable conformational changes were observed in the C-terminal domain as indicated by the lack of significant amide proton-nitrogen chemical shift perturbations (Fig. 1B). This strongly supports that CyaA-ACD association prevents Ca^{2+}/Mg^{2+} exchange in C-terminal CaM by increasing Ca^{2+} affinity. Even in the presence of excess Mg^{2+} concentrations, Ca^{2+} remained bound to sites III and IV in the $2Mg^{2+}/2Ca^{2+}$-loaded CaM/CyaA-ACD complex. These findings are significant because they point to the possibility that even in the resting state, when cytosolic Ca^{2+} concentrations are low, $2Mg^{2+}/2Ca^{2+}$-loaded CaM/CyaA-ACD is likely to be the predominant conformer in the cell.

CyaA-ACD binding to CaM not only affects its conformation but it also impacts metal binding properties. We observed that when CyaA-ACD and Ca^{2+} are bound to the C-terminal domain, site II of CaM exhibited a structurally unique conformation in the $2Mg^{2+}/2Ca^{2+}$-loaded state as compared to the free $4Mg^{2+}$-CaM (Fig. 2A). Most notably, a more substantial chemical shift difference was observed between $4Mg^{2+}$-CaM and $2Mg^{2+}/2Ca^{2+}$-CaM/CyaA-ACD for T62 in site II as compared to T26, the corresponding peak in site I. It is possible that CyaA-ACD association with CaM increases Mg^{2+} binding affinity at site II which results in more pronounced chemical shift perturbations (Fig. 2B). Further evidence supporting that CyaA-ACD association modulates the metal binding properties of CaM is seen by comparing other regions of NMR spectra of $4Mg^{2+}$-CaM, $2Mg^{2+}/2Ca^{2+}$-CaM, and $2Mg^{2+}/2Ca^{2+}$-CaM/CyaA-ACD. The 2D correlation spectra of $4Mg^{2+}$-CaM and $2Mg^{2+}/2Ca^{2+}$-CaM demonstrate that distinct amide proton-nitrogen chemical shifts are observed in each metal-bound state (Fig. 3A, B respectively). For example, peaks T29, D58, and T117 mapping to sites I, II, and III, respectively, had chemical shifts which are consistent with CaM being in the $4Mg^{2+}$-loaded state (Fig. 3A). In the $2Mg^{2+}/2Ca^{2+}$-CaM sample, the amide nitrogen of T117 was shifted +1.5 p.p.m. as compared to $4Mg^{2+}$-CaM and this position in the spectrum was comparable to that the observed in the Ca^{2+}-loaded state, indicating C-terminal-specific Ca^{2+} binding (Fig. 3A, B). However, significant exchange broadening was observed for the amide proton-nitrogen resonances of T29 and D58 in $2Mg^{2+}/2Ca^{2+}$-CaM as compared to $4Mg^{2+}$-CaM, but no peaks corresponding to Ca^{2+}-loaded protein were observed for any N-terminal resonances, indicating that Mg^{2+} binding is site-specific, with conformational exchange occurring between the Mg^{2+}-free and Mg^{2+}-bound states (Fig. 3B). Unfortunately, significant exchange broadening of these N-terminal resonances in CaM precluded the determination of apparent Mg^{2+} binding affinities by NMR. Unexpectedly, the association of CyaA-ACD with the C-terminal domain of CaM reduced Mg^{2+} exchange at sites I and II in the N-terminal domain as evidenced by the lack of exchanged broadened peaks (Fig. 3C). In the presence of 40 mM Mg^{2+}, the amide proton-nitrogen resonances of T29 and D58 reappeared and were readily detectable in the spectrum of the $2Mg^{2+}/2Ca^{2+}$-CaM/CyaA-ACD complex, which suggests that CyaA-ACD binding to C-terminal CaM modulates metal exchange most likely by increasing Mg^{2+} binding affinities in the N-terminal domain. To the best of our knowledge,

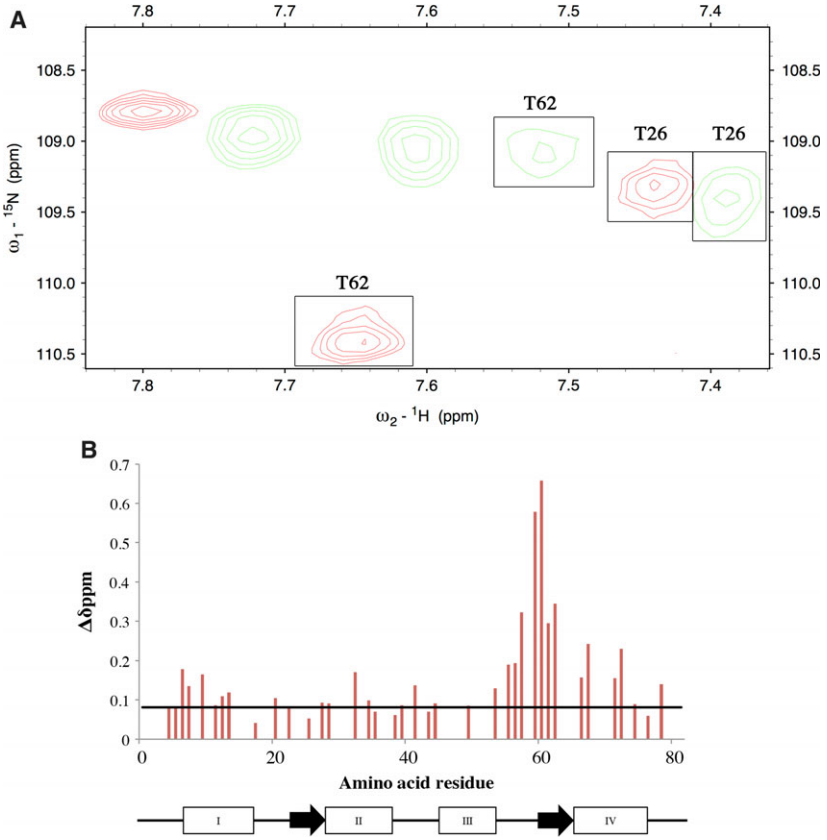

Fig. 2. 2D ^{1}H-^{15}N TROSY spectra demonstrating that the metal binding properties at site II are affected by the presence of CyaA and Ca^{2+} binding in the C terminus of CaM. (A) [^{15}N, ^{13}C, ^{2}H]-CaM free in the $4Mg^{2+}$saturation (red) and [^{15}N, ^{13}C, ^{2}H]-CaM bound to CyaA-ACD in the presence of $2Mg^{2+}/2Ca^{2+}$ saturation (green). (B) Amide proton-nitrogen chemical shift differences between $2Mg^{2+}/2Ca^{2+}$-CaM/CyaA and $4Mg^{2+}$-CaM. Selected residues are labeled according to the amino acid residue. The secondary structure of CaM is summarized with rectangles (helices) and arrows (β-sheets). The average chemical shift change + one standard deviation is indicated by the horizontal black line. The interaction of CyaA-ACD with the C-terminal domain of CaM induces chemical shift perturbations at site II in the N-terminal domain of CaM. It is possible that CyaA-ACD-induced conformational modulation of site II might increase Mg^{2+} binding affinity in the N-terminal domain of CaM.

this is the first report of an allosteric interdomain communication pathway specific to CyaA-ACD binding that functions in fine-tuning the Mg^{2+} and Ca^{2+} binding affinities in CaM.

Global conformational analyses of $4Ca^{2+}$-CaM/CyaA-ACD and $2Mg^{2+}/2Ca^{2+}$-CaM/CyaA-ACD complexes

Dynamic light scaterring has been previously used to examine the global conformation of CaM and CaM/CyaA-ACD complexes [19] under various conditions. In DLS, the hydrodynamic diameters are determined from the Stokes–Einstein equation based on the presence of a sphere. Measurement of the hydrodynamic diameter of a rod-shaped protein results in a larger value as compared to that determined for a sphere of similar molecular mass. Previous hydrodynamic studies of the CaM/CyaA-ACD complex demonstrated that it has an ellipsoid conformation instead of a globular shape in solution [19,29]. In the present study, all samples of CaM and CaM/CyaA-ACD were determined to be monodisperse and free of aggregation (Fig. 4). The hydrodynamic diameter of $4Ca^{2+}$-CaM/CyaA-ACD increased as compared to free $4Ca^{2+}$-CaM (Fig. 4), which indicates the presence of binary complex formation. Comparison of the hydrodynamic diameters of the $4Ca^{2+}$-CaM/CyaA-ACD to $2Mg^{2+}/2Ca^{2+}$-CaM/CyaA-ACD, revealed that the metal-bound complexes have similar global conformations in solution. These findings are consistent with the formation of an elongated CaM/CyaA-ACD complex [17,19,29]. While the $4Ca^{2+}$-CaM/CyaA-ACD has been identified as being oblong in solution, this is the first known report of an extended, partially Mg^{2+}-loaded conformation for the CaM/CyaA-ACD complex.

Native PAGE analyses further supported that the $4Ca^{2+}$-CaM/CyaA-ACD and $2Mg^{2+}/2Ca^{2+}$-CaM/CyaA-ACD have comparable global conformations (Fig. 5A). The $4Ca^{2+}$-CaM/CyaA-ACD and $2Mg^{2+}/2Ca^{2+}$ CaM/CyaA-ACD complexes exhibited similar native PAGE migration patterns, hence, based on previous data demonstrating that $4Ca^{2+}$-CaM/CyaA-ACD is extended, the $2Mg^{2+}/2Ca^{2+}$ CaM/CyaA-ACD complex is regarded to have an elongated global conformation. These findings are in agreement with reports from Karst *et al.* [29] that CaM/CyaA-ACD is elongated and that the conformation of free CyaA-ACD differs from that in the complex. We have

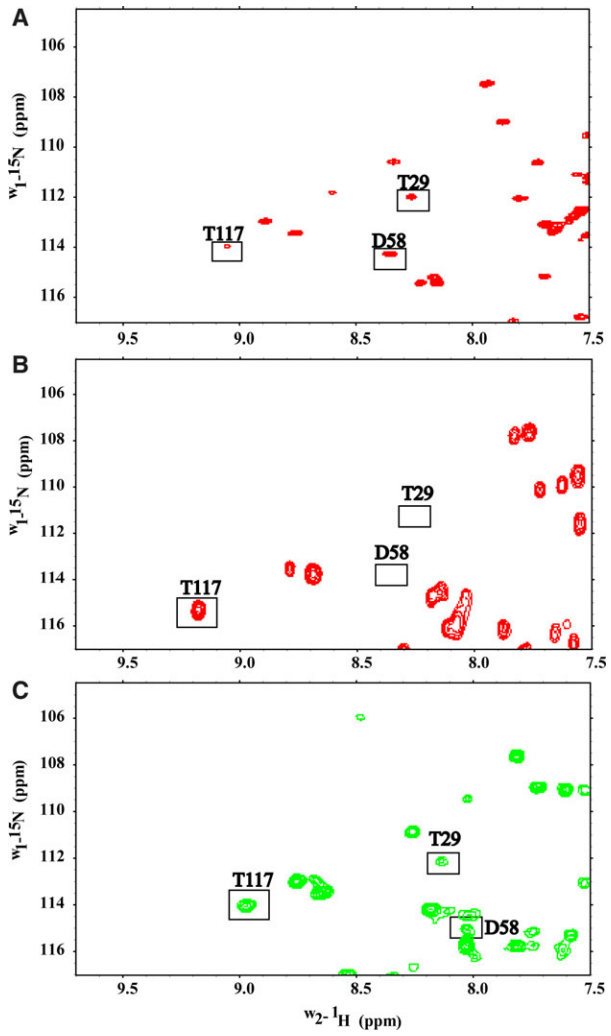

Fig. 3. CyaA-ACD interaction with CaM stabilizes CaM metal binding in the N terminus of CaM. Selected regions of 2D amide proton-nitrogen correlation spectra are displayed for (A) [^{15}N, ^{13}C, ^{2}H]-CaM-free $4Mg^{2+}$ saturation (red), (B) [^{15}N, ^{13}C, ^{2}H]-CaM-free $2Mg^{2+}/2Ca^{2+}$ saturation (dark red), (C) [^{15}N, ^{13}C, ^{2}H]-CaM/CyaA $2Mg^{2+}/2Ca^{2+}$ saturation (green). The C-terminal domain of CaM has distinct Mg^{2+}- and Ca^{2+}-loaded conformations as evidenced by the position of T117 in site III. In the absence of CyaA-ACD, CaM residues T29 and D58 are broadened in the $2Mg^{2+}/2Ca^{2+}$-loaded state due to Mg^{2+} exchange. Upon CyaA-ACD association, the exchange broadening at sites I and II in CaM diminished, which is likely the consequence of increased apparent Mg^{2+} binding affinity induced by CyaA-ACD association.

demonstrated that CyaA-ACD interaction with both domains of CaM is necessary to maintain the complex in an extended global state [19]. In that same study, we found that disruption of intermolecular contacts between the β-hairpin of CyaA and CaM decreases the hydrodynamic radius of the complex. Based on these findings, we proposed that mutation of site I in CaM,

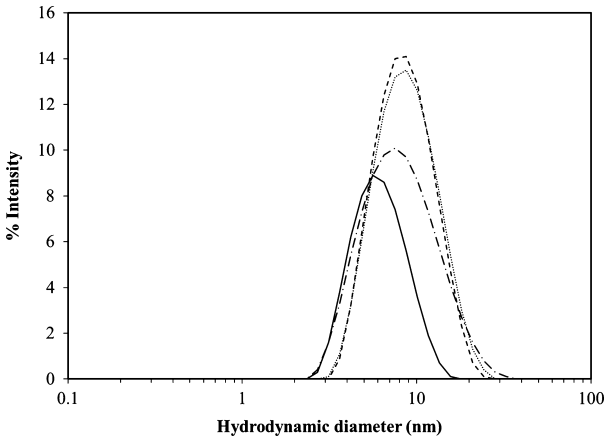

Fig. 4. Dynamic light scattering experiments show that the hydrodynamic diameters of CaM/CyaA-ACD complexes are larger than those measured for free CaM. The intensity versus the hydrodynamic diameter are plotted for free $4Ca^{2+}$-CaM (solid black line), $4Ca^{2+}$-CaM/CyaA-ACD (dashed line), $2Mg^{2+}/2Ca^{2+}$-CaM/CyaA-ACD (dotted line), and $2Mg^{2+}/2Ca^{2+}$-CaM(E31D)/CyaA-ACD (dashed/dotted line). The reduction in the hydrodynamic diameter of $2Mg^{2+}/2Ca^{2+}$-CaM(E31D)/CyaA-ACD as compared to $2Mg^{2+}/2Ca^{2+}$-CaM/CyaA-ACD provides evidence that this mutant induces a global compaction in this complex.

in particular, modification in side-chains that are likely to be located at the protein–protein binding interface, would also impact the global conformation of CaM/CyaA in the presence of Ca^{2+} and Mg^{2+} saturation. To test this prediction, we generated CaM(E31D) and examined its metal-dependent association with CyaA-ACD.

Global conformational change in the $2Mg^{2+}/2Ca^{2+}$-CaM(E31D)/CyaA-ACD complex

With the CaM(E31D) mutant, our goal was to examine CyaA–ACD interaction using a CaM mutant that was not likely to have substantial conformational changes and was Mg^{2+} specific at site I. The −Z ligand in the metal-binding loops of canonical EF-hand proteins, such as CaM and TnC, are Glu acid residues. In Ca^{2+}-loaded CaM, Oε1 and Oε2 of Glu residues coordinate the Ca^{2+} ion in a bidentate fashion. However, in Mg^{2+}-loaded CaM these side-chain groups do not participate in Mg^{2+} coordination [12,22]. This is in direct contrast to TnC, which has monodentate ligation of the Mg^{2+} ion mediated through Oε1 of Glu in the presence of target peptide [11,30]. TnC has been demonstrated to undergo a compaction in of the metal-binding loops in the Mg^{2+}-loaded state [11], whereas CaM does not coordinate Mg^{2+} through the −Z ligand, so metal ligation is

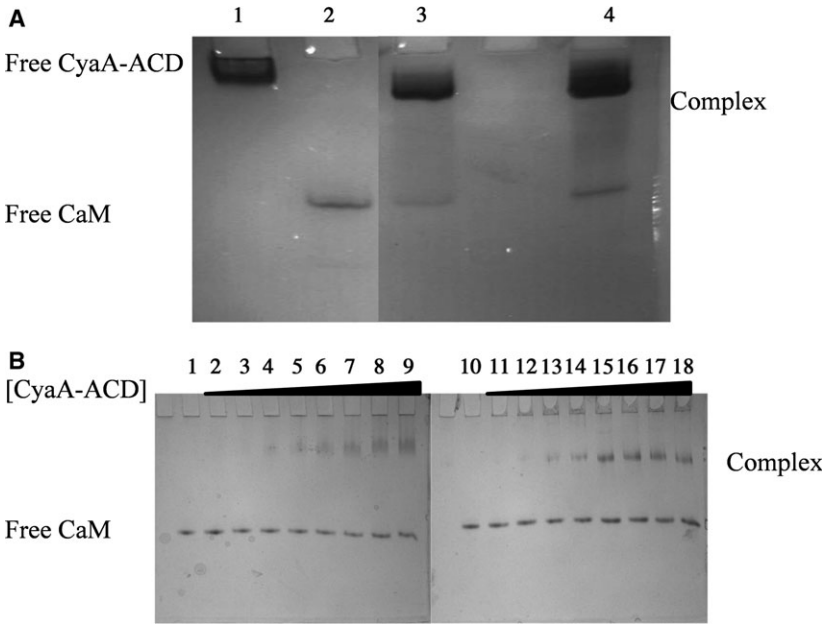

Fig. 5. Complex formation between CaM and CyaA-ACD in the presence of Ca^{2+} or Mg^{2+}/Ca^{2+} saturation can be monitored by native PAGE. Following SEC, complexes were visualized using native 15% PAGE and Coomassie Brilliant blue staining. (A) (Lane 1) CyaA-ACD, (Lane 2) CaM, (Lane 3) $4Ca^{2+}$-CaM/CyaA-ACD, (Lane 4) $2Mg^{2+}/2Ca^{2+}$-CaM/CyaA-ACD. The electrophoretic mobility of complexes consisting of $4Ca^{2+}$-CaM/CyaA-ACD or $2Mg^{2+}/2Ca^{2+}$-CaM/CyaA-ACD was intermediate as compared to free CaM and free CyaA. A similar shift in mobility was observed for $4Ca^{2+}$-CaM/CyaA-ACD or $2Mg^{2+}/2Ca^{2+}$-CaM/CyaA-ACD suggesting that these complexes have comparable shapes and charges. (B) Titration studies were performed with varying amounts of CyaA-ACD (0–2.5 μM) added to 5 μM of $4Ca^{2+}$-CaM or $2Mg^{2+}/2Ca^{2+}$-CaM(E31D). (Lane 1) Free $4Ca^{2+}$-CaM, (Lanes 2–9) increasing amounts of CyaA-ACD (Lane 10) Free $2Mg^{2+}/2Ca^{2+}$-CaM(E31D), (Lanes11–18) increasing amounts of CyaA-ACD. The mutant $2Mg^{2+}/2Ca^{2+}$-CaM(E31D)/CyaA-ACD complex had an increased electrophoretic mobility which indicates it is compacted as compared to the $4Ca^{2+}$ or $2Mg^{2+}/2Ca^{2+}$-loaded states.

limited to the N-terminal portion of the loop [12,22]. Metal binding specificity can be controlled by the amino acid side-chain present at position 12 of the EF-hand loop. In other EF-hand proteins, mutation of the Glu residue at the −Z position to Asp has been shown to promote Mg^{2+} binding specificity without inducing substantial conformational changes in the proteins [31,32].

In this study, CaM(E31D) was engineered in order to optimize the Mg^{2+} binding properties at site I, without invoking a charge change at the −Z ligand, so that we would minimize the possibility of disrupting intermolecular association with CyaA-ACD. We used DLS and native PAGE analyses to assess the structural consequences of mutant CaM(E31D) on CyaA-ACD association. We expect CaM(E31D) to be Mg^{2+} specific at site I while site II is capable of Mg^{2+} or Ca^{2+} coordination. Surprisingly, we observed that mutation at this position increased the degree of compaction in $2Mg^{2+}/2Ca^{2+}$-CaM(E31D)/CyaA-ACD, which results in a reduction in the hydrodynamic diameter from 9 nm in the $2Mg^{2+}/2Ca^{2+}$-CaM/CyaA-ACD complex to 7.5 nm in the mutant $2Mg^{2+}/2Ca^{2+}$-CaM (E31D)/CyaA-ACD complex (Fig. 4). Similarly, the electrophoretic mobility of the $2Mg^{2+}/2Ca^{2+}$-CaM (E31D)/CyaA-ACD complex was altered as compared to $4Ca^{2+}$CaM/CyaA-ACD or $2Mg^{2+}/2Ca^{2+}$CaM/CyaA-ACD, which supports that this mutant complex most likely has a different global shape (Fig. 5B). Taken together, these data suggest that alteration of the −Z ligand disrupts the intermolecular associations needed for formation of an extended Mg^{2+}-loaded CaM/CyaA-ACD complex. Previously, we reported the existence of intermolecular association between site I in CaM and CyaA-ACD that contributes to the extended global conformation [19]. Based on the observations in our current work, we concluded that site I mutation results in the loss of stabilizing interactions between N-terminal CaM and CyaA-ACD in the $2Mg^{2+}/2Ca^{2+}$-CaM/CyaA-ACD complex. These data point to a model of CaM-dependent activation of CyaA-ACD that requires an extended complex conformation similar to that observed for *B. anthracis* EF [14]. It is interesting to speculate that this extended conformation

mechanism in CaM/CyaA-ACD might also be one that permits the modification of metal binding in CaM. While the role of CyaA-ACD binding in the modulation of CaM's metal binding properties remains unclear, it is likely to contribute to enzyme activation by desensitizing the system to fluctuations in intracellular Ca^{2+} levels.

In summary, comparing $4Ca^{2+}$-CaM/CyaA-ACD to $2Mg^{2+}/2Ca^{2+}$-CaM/CyaA-ACD reveals that Mg^{2+} binding is localized to sites I and II of N-terminal CaM. Interaction with CyaA-ACD increases the apparent Ca^{2+} binding in C-terminal CaM as evidenced by prohibited metal exchange in the CaM/CyaA-ACD complex. The presence of CyaA-ACD and Ca^{2+} binding to C-CaM modulates site II of Mg^{2+}-CaM. In the absence of an effector, N-terminal CaM residues are prone to broadening, however, the presence of CyaA-ACD reduces Mg^{2+} exchange in N-terminal CaM. DLS data show similarities between $4Ca^{2+}$-CaM/CyaA-ACD and $2Mg^{2+}/2Ca^{2+}$-CaM/CyaA-ACD global conformations of these complexes. In comparison to other prokaryotic adenylate cyclase toxins, such as EF from *Bacillus anthracis* and ExoY from *Pseudomonas aeruginosa*, there is only 25% sequence identity at the amino acid level with respect to the ATP-binding domain. While the host cell activator is unknown for ExoY, EF and CyaA-ACD are both CaM-dependent and have evolved molecular mechanisms for activation that are distinct from eukaryotic adenylate cyclases. Taken together, these data indicate that CyaA-ACD binding likely modulates metal binding to CaM. The molecular role CyaA-ACD plays in fine-tuning CaM's metal binding capabilities remains to be determined. High-resolution structures of the CaM/CyaA-ACD complexes in the Ca^{2+}- and Mg^{2+}-loaded states are necessary in order to understand the structural mechanisms by which of prokaryotic adenylate cyclase toxins are controlled.

Acknowledgements

We gratefully acknowledge the contribution of Dr Andor Kiss in supervising and maintaining the instrumentation in the Center for Bioinformatics and Functional Genomics (CBFG). Also, we would like to express our gratitude to Xiaoyun Deng for her technical assistance in the CBFG. We thank Drs Sameer Al-Wahid and Theresa Ramelot for maintaining the NMR spectrometers. This work was supported by CFR (NLF) and DUOS (TIS, NLF) grants from Miami University. NLF is also supported in part by USDA project number 6034-22000-041-24.

Author contributions

TIS, CCE, CWJ, and NLF performed the experiments, analyzed data, and interpreted results. TIS and NLF wrote the manuscript. All authors provided comments and edits in the development of the manuscript.

References

1 Ladant D, Michelson S, Sarfati R, Gilles AM, Predeleanu R and Barzu O (1989) Characterization of the calmodulin-binding and of the catalytic domains of *Bordetella pertussis* adenylate cyclase. *J Biol Chem* **264**, 4015–4020.

2 Rose T, Sebo P, Bellalou J and Ladant D (1995) Interaction of calcium with *Bordetella pertussis* adenylate cyclase toxin. Characterization of multiple calcium-binding sites and calcium-induced conformational changes. *J Biol Chem* **270**, 26370–26376.

3 Wolff J, Cook GH, Goldhammer AR and Berkowitz SA (1980) Calmodulin activates prokaryotic adenylate cyclase. *Proc Natl Acad Sci USA* **77**, 3841–3844.

4 Weiss AA and Goodwin MS (1989) Lethal infection by *Bordetella pertussis* mutants in the infant mouse model. *Infect Immun* **57**, 3757–3764.

5 Weingart CL, Mobberley-Schuman PS, Hewlett EL, Gray MC and Weiss AA (2000) Neutralizing antibodies to adenylate cyclase toxin promote phagocytosis of *Bordetella pertussis* by human neutrophils. *Infect Immun* **68**, 7152–7155.

6 Shen Y, Lee YS, Soelaiman S, Bergson P, Lu D, Chen A, Beckingham K, Grabarek Z, Mrksich M and Tang WJ (2002) Physiological calcium concentrations regulate calmodulin binding and catalysis of adenylyl cyclase exotoxins. *EMBO J* **21**, 6721–6732.

7 Strynadka NC and James MN (1989) Crystal structures of the helix-loop-helix calcium-binding proteins. *Annu Rev Biochem* **58**, 951–998.

8 Ikura M, Clore GM, Gronenborn AM, Zhu G, Klee CB and Bax A (1992) Solution structure of a calmodulin-target peptide complex by multidimensional NMR. *Science* **256**, 632–638.

9 Ohki S, Ikura M and Zhang M (1997) Identification of Mg^{2+}-binding sites and the role of Mg^{2+} on target recognition by calmodulin. *Biochemistry* **36**, 4309–4316.

10 Ohashi W, Hirota H and Yamazaki T (2011) Solution structure and fluctuation of the $Mg(^{2+})$-bound form of calmodulin C-terminal domain. *Protein Sci* **20**, 690–701.

11 Finley NL, Howarth JW and Rosevear PR (2004) Structure of the Mg^{2+}-loaded C-lobe of cardiac troponin C bound to the N-domain of cardiac troponin I: comparison with the Ca^{2+}-loaded structure. *Biochemistry* **43**, 11371–11379.

12 Senguen FT and Grabarek Z (2012) X-ray structures of magnesium and manganese complexes with the N-

terminal domain of calmodulin: insights into the mechanism and specificity of metal ion binding to an EF-hand. *Biochemistry* **51**, 6182–6194.
13 Jurado LA, Chockalingam PS and Jarrett HW (1999) Apocalmodulin. *Physiol Rev* **79**, 661–682.
14 Drum CL, Yan SZ, Bard J, Shen YQ, Lu D, Soelaiman S, Grabarek Z, Bohm A and Tang WJ (2002) Structural basis for the activation of anthrax adenylyl cyclase exotoxin by calmodulin. *Nature* **415**, 396–402.
15 Ulmer TS, Soelaiman S, Li S, Klee CB, Tang WJ and Bax A (2003) Calcium dependence of the interaction between calmodulin and anthrax edema factor. *J Biol Chem* **278**, 29261–29266.
16 Shen Y, Zhukovskaya NL, Guo Q, Florian J and Tang WJ (2005) Calcium-independent calmodulin binding and two-metal-ion catalytic mechanism of anthrax edema factor. *EMBO J* **24**, 929–941.
17 Guo Q, Shen Y, Lee YS, Gibbs CS, Mrksich M and Tang WJ (2005) Structural basis for the interaction of *Bordetella pertussis* adenylyl cyclase toxin with calmodulin. *EMBO J* **24**, 3190–3201.
18 Selwa E, Laine E and Malliavin TE (2012) Differential role of calmodulin and calcium ions in the stabilization of the catalytic domain of adenyl cyclase CyaA from *Bordetella pertussis*. *Proteins* **80**, 1028–1040.
19 Springer TI, Goebel E, Hariraju D and Finley NL (2014) Mutation in the beta-hairpin of the *Bordetella pertussis* adenylate cyclase toxin modulates N-lobe conformation in calmodulin. *Biochem Biophys Res Commun* **453**, 43–48.
20 Guo Q, Jureller JE, Warren JT, Solomaha E, Florian J and Tang WJ (2008) Protein-protein docking and analysis reveal that two homologous bacterial adenylyl cyclase toxins interact with calmodulin differently. *J Biol Chem* **283**, 23836–23845.
21 Tjandra N, Kuboniwa H, Ren H and Bax A (1995) Rotational dynamics of calcium-free calmodulin studied by ^{15}N-NMR relaxation measurements. *Eur J Biochem* **230**, 1014–1024.
22 Malmendal A, Evenas J, Thulin E, Gippert GP, Drakenberg T and Forsen S (1998) When size is important. Accommodation of magnesium in a calcium binding regulatory domain. *J Biol Chem* **273**, 28994–29001.
23 Delaglio F, Grzesiek S, Vuister GW, Zhu G, Pfeifer J and Bax A (1995) NMRPipe: a multidimensional spectral processing system based on UNIX pipes. *J Biomol NMR* **6**, 277–293.
24 Goddard TD and Kneller DG (2008) Sparky-NMR Assignment and Integration Software, Sparky 3.
25 Biekofsky RR, Martin SR, Browne JP, Bayley PM and Feeney J (1998) Ca^{2+} coordination to backbone carbonyl oxygen atoms in calmodulin and other EF-hand proteins: 15N chemical shifts as probes for monitoring individual-site Ca^{2+} coordination. *Biochemistry* **37**, 7617–7629.
26 Vigil D, Gallagher SC, Trewhella J and Garcia AE (2001) Functional dynamics of the hydrophobic cleft in the N-domain of calmodulin. *Biophys J* **80**, 2082–2092.
27 Tripathi S and Portman JJ (2009) Inherent flexibility determines the transition mechanisms of the EF-hands of calmodulin. *Proc Natl Acad Sci USA* **106**, 2104–2109.
28 Zhang M, Abrams C, Wang L, Gizzi A, He L, Lin R, Chen Y, Loll PJ, Pascal JM and Zhang JF (2012) Structural basis for calmodulin as a dynamic calcium sensor. *Structure* **20**, 911–923.
29 Karst JC, Sotomayor Perez AC, Guijarro JI, Raynal B, Chenal A and Ladant D (2010) Calmodulin-induced conformational and hydrodynamic changes in the catalytic domain of *Bordetella pertussis* adenylate cyclase toxin. *Biochemistry* **49**, 318–328.
30 Finley N, Dvoretsky A and Rosevear PR (2000) Magnesium-calcium exchange in cardiac troponin C bound to cardiac troponin I. *J Mol Cell Cardiol* **32**, 1439–1446.
31 Cates MS, Berry MB, Ho EL, Li Q, Potter JD and Phillips GN Jr (1999) Metal-ion affinity and specificity in EF-hand proteins: coordination geometry and domain plasticity in parvalbumin. *Structure* **7**, 1269–1278.
32 Zhang J, Shettigar V, Zhang GC, Kindell DG, Liu X, Lopez JJ, Yerrimuni V, Davis GA and Davis JP (2011) Engineering parvalbumin for the heart: optimizing the Mg binding properties of rat beta-parvalbumin. *Front Physiol* **2**, 77.